Check for updates

[ASr₄Cl][Ge₃S₁₀] (A = Na, K) and [KBa₄Cl][Ge₃S₁₀]: new salt-inclusion infrared nonlinear optical crystals with zero-dimensional [Ge₃S₉] clusters†

Yufei Song, Shaoxin Cui, Zhen Qian, Hongwei Yu, Zhanggui Hu, Jiyang Wang, Yicheng Wu and Hongping Wu [ORCID] *

Three new chalcohalide nonlinear optical crystals, [ASr₄Cl][Ge₃S₁₀] (A = Na, K) and [KBa₄Cl][Ge₃S₁₀], have been successfully designed and synthesized by combining the covalent [Ge₃S₉] clusters and ionic [AB₄Cl] frameworks. Their crystal structures were determined by single crystal X-ray diffraction, which showed that all three compounds crystallized in the noncentrosymmetric and polar space group of $P6_3$. Three structures are iso-structural and can be seen as salt-inclusion structures with the isolated [Ge₃S₉] clusters stacked alternately along the c axis and $^1_\infty[\text{ClNaSr(2)}_3]^{6+}$ chains acting as scissors to cut the connection between the [Ge₃S₉] clusters, which is still rare in the known chalcohalides. The IR and Raman spectra indicate that [ASr₄Cl][Ge₃S₁₀] (A = Na, K) and [KBa₄Cl][Ge₃S₁₀] have wide IR transparent windows up to 20 μm. UV-Vis-NIR diffuse reflectance spectra manifest that all three compounds have large band gaps of 3.54, 3.51, and 3.57 eV, respectively. In addition, the title compounds also exhibit large laser damage thresholds (~12 × AgGaS₂) and moderate SHG responses (1.08, 0.91, and 0.82 × AgGaS₂, respectively). These properties demonstrate their potential as IR NLO crystals. Furthermore, the influence of the (M + N)/Q ratios (M = IIIA or IVA, N = IB or IIB or cations coordinated as [MₓQᵧ] anionic groups; Q = S, Se) on the anionic group structural dimensions was discussed, and the structure–property relationship was also studied based on the first-principles calculations. These may produce some insights for designing new chalcohalides.

Tianjin Key Laboratory of Functional Crystal Materials, Institute of Functional Crystal, Tianjin University of Technology, Tianjin 300384, China.
E-mail: wuhp@ms.xjb.ac.cn

†Electronic supplementary information (ESI) available: Atomic coordinates, equivalent isotropic displacement parameters, and the bond valence sums of each atom; selected distances and angles; experimental and calculated XRD patterns; elemental analysis; IR transmission; and dipole moment calculations. CCDC 2190986, 2190987 and 2201923. For ESI and crystallographic data in CIF or other electronic format see DOI: https://doi.org/10.1039/d2qi01689c

Introduction

Mid-infrared coherent light sources covering the atmospheric windows of 3–5 and 8–12 μm have many important applications in the fields of industry and the military, such as atmospheric monitoring, remote sensing, and IR countermeasures. However, it is difficult or even impossible for solid-state lasers to directly radiate MIR coherent light sources owing to the deficiency of viable laser crystals.[1–4] In contrast, adopting the frequency conversion on nonlinear optical crystals, such as optical parametric oscillation, optical parametric amplification and difference frequency generation, is the best way to obtain different MIR coherent radiation sources. As a result, NLO crystals are the key components of solid-state lasers, which will directly determine the spectral regions or even the highest output energies the lasers can achieve.[5–8] During the past decades, a series of excellent oxide-based NLO crystals have been successfully synthesized and some of them have been commercialized. But most of them cannot be used in the IR region due to the insufficient optical transparency and small second-harmonic generation response. Therefore, designing new IR nonlinear optical crystals is still the current research interest.

An ideal IR nonlinear optical crystal needs to satisfy the following strict property requirements, including crystallographically noncentrosymmetric structures, large second-harmonic generation responses (>0.5 × AgGaS₂), wide transparent regions (3–14 μm), suitable birefringence as well as large band gap (E_g > 3.0 eV) and high laser damage threshold (>10 × AgGaS₂). Metal chalcogenides can act as excellent candidates to develop novel IR nonlinear optical materials due to their abundant structural features and excellent optical performances including broad optical transparency and strong SHG responses, *e.g.* chalcopyrite-type chalcogenides, AgGaS₂,[9]

5932 | *Inorg. Chem. Front.*, 2022, **9**, 5932–5940

This journal is © the Partner Organisations 2022

AgGaSe$_2$,[10] and ZnGeP$_2$ [11] are also the currently main IR nonlinear optical crystals. But notably, large second-harmonic generation responses and wide band gaps usually conflict in chalcogenides.[12] This has resulted in the low laser damage threshold or two-photon absorption, which has become the major obstacle to their broader applications, especially under high-power conditions. However, recent research shows combining the multiple anionic groups in one compound can better balance the above properties' conflict.[13–19] In particular, combination of polarizable Q^{2-} (Q = S, Se, Te) and large electronegative X$^-$ (X = F, Cl, Br) anions has resulted in many interesting heteroanionic IR nonlinear optical crystals with large second-harmonic generation responses and band-gaps, e.g. [ABa$_2$Cl][Ga$_4$S$_8$] (A = Rb, Cs) (0.9 × AgGaS$_2$, 3.30 eV),[20] Ba$_3$AGa$_5$Se$_{10}$Cl$_2$ (A = Cs, Rb, K) (1.0 × AgGaS$_2$, 3.25 eV),[21] Ba$_4$ZnGa$_5$S$_{10}$Cl$_2$ (1.1 × AgGaS$_2$, 3.85 eV),[12] Ba$_4$Ge$_3$S$_9$Cl$_2$ (2.4 × AgGaS$_2$, 2.91 eV),[22] etc. Structurally, these compounds can all be seen as halide-salt-inclusion chalcogenides, where the covalent chalcogenide lattices are in charge of a large second-harmonic generation response while the ionic halide lattices are responsible for a wide band-gap. The fine mixing of the covalent and ionic bonds in the structure have been considered to be an effective strategy for the design of excellent IR nonlinear optical materials.[23,24]

Guided by the above ideas, we have focused our research interests on the A/B/Ge/S/Cl (A = alkali, B = alkaline-earth metal) system, where there are few compounds reported.[25,26] After continuous attempts, three new salt-inclusion chalcogenides, [ASr$_4$Cl][Ge$_3$S$_{10}$] (A = Na, K) and [KBa$_4$Cl][Ge$_3$S$_{10}$], have been successfully synthesized by the flux method. They all crystallize in the noncentrosymmetric and polar hexagonal space group $P6_3$, and they exhibit isolated [Ge$_3$S$_9$] rings and $^1_\infty$[ClNaSr(2)$_3$]$^{6+}$ chains, which are rarely reported in the known chalcohalides. The experimental and theoretical analyses revealed that [ASr$_4$Cl][Ge$_3$S$_{10}$] (A = Na, K) and [KBa$_4$Cl][Ge$_3$S$_{10}$] achieve the optimal balance among the critical but far difficult to reconcile demands, including wide infrared transmission ranges (2–20 μm), wide band gaps (3.51–3.57 eV), large laser damage threshold values (~12 × AgGaS$_2$), and moderate second-harmonic generation responses (0.82–1.08 × AgGaS$_2$). Herein, we will report their syntheses, crystal structures, optical properties, and structure–property relationships.

Experimental section

Materials

NaCl (99.5%), KCl (99.5%), SrS (99.99%), BaS (99.9%), Ge (99.99%) and S (99.9%) were purchased from Fuchen (Tianjin) Chemical Reagent Co. Ltd, Shanghai Aladdin Biochemical Technology Co. Ltd, and Beijing Hawk Science and Technology Co. Ltd (China), respectively.

Syntheses

All the starting materials were used as purchased and stored in a glovebox filled with purified Ar (moisture and oxygen levels are less than 0.1 ppm), and all manipulations were performed inside the glovebox. The crystals of [ASr$_4$Cl][Ge$_3$S$_{10}$] (A = Na, K) and [KBa$_4$Cl][Ge$_3$S$_{10}$] were prepared with a mixture of NaCl (KCl), SrS (BaS), Ge, and S in ratios of NaCl:SrS:Ge:S = 1:4:3:6, KCl:SrS:Ge:S = 1:4:3:6, and KCl:BaS:Ge:S = 1:4:3:6, respectively. Then the mixtures were loaded in fused silica tubes under a vacuum of 10^{-3} Pa. Next, these fused silica tubes were placed in a furnace and annealed at 1223 K for 50 h and then kept at this temperature for 100 h to ensure that the mixtures completely melted. This was followed by slowly cooling at 3 K h^{-1} to 473 K, and then the furnace was turned off. Anhydrous ethanol and N,N-dimethylformamide (DMF) were used to wash the reaction products for removing the other byproducts. Finally, their crystals were obtained. The approximate yields of these crystals are about 100%. These compounds were all stable in the air for several months.

Polycrystalline samples of the above compounds could be easily synthesized by heating stoichiometric mixtures sealed in an evacuated silica tube at 1123 K for 2 days. The samples melted into smooth balls, and the uniformity between the powder X-ray diffraction (PXRD) patterns of as-synthesized samples and simulated patterns indicated the high purity of the target samples.

Structural refinement and crystal data

Single crystal XRD data were collected on a Bruker SMART APEX II CCD single crystal diffractometer at room temperature with Mo Kα radiation (λ = 0.71073 Å). The collected data were integrated using the SAINT program.[27] The data were analyzed and refined using the SHELXS program to obtain the final crystal structure data.[28,29] The final structures were checked with PLATON,[30] and no other higher symmetry elements were found. The crystallographic data and structure refinements are presented in Table 1. The atomic coordinates, equivalent isotropic atomic displacement parameters, the bond valence calculations for all atoms, and the selected distances (Å) and angles (°) are summarized in Tables S2 and S3.†

Powder X-ray diffraction (PXRD)

The PXRD data were collected using a SmartLab 9KW X-ray diffractometer at room temperature (Cu Kα radiation) with scanning ranges of 10–70° for [ASr$_4$Cl][Ge$_3$S$_{10}$] (A = Na, K) and [KBa$_4$Cl][Ge$_3$S$_{10}$] in 2θ and a scan step of 2° min^{-1}. The measurement results show that the PXRD patterns of the as-synthesized samples match the calculated ones derived from their single crystal data (Fig. S1†).

Energy-dispersive spectroscopy (EDS)

Microprobe elemental analyses and the elemental distribution mapping were performed using a field-emission scanning electron microscope (Quanta FEG 250) made by FEI. The EDS experiment indicates that the average atomic ratio of Na (K), Sr (Ba), Ge, S, and Cl is 5.13%–5.37% : 19.22%–20.72% : 15.50%–16.39% : 51.09–53.28% : 5.80%–6.62% for [ASr$_4$Cl][Ge$_3$S$_{10}$] (A = Na, K) and [KBa$_4$Cl][Ge$_3$S$_{10}$], respectively, which are approximately equal to the theoretical ones (Fig. S2†).

This journal is © the Partner Organisations 2022

Inorg. Chem. Front., 2022, 9, 5932–5940 | 5933

Table 1 Property comparison of compounds with related chalcohalides

Compounds	Space group	E_g (eV)	Second-harmonic generation response (× AgGaS$_2$)	Δn or PM/NPM	Anionic group dimensions	Ref.
Li$_2$Cs$_2$Ga$_3$S$_6$Cl	$Pna2_1$	4.18	0.7	PM	3D	47
Ba$_4$ZnGa$_4$S$_{10}$Cl$_2$	$I\bar{4}$	3.85	1.1	0.012/PM	3D	12
ABa$_3$Ga$_5$S$_{10}$Cl$_2$ (A = Cs, Rb, K)	$I\bar{4}$	3.93	0.9	0.008/PM	3D	48
ABa$_3$Ga$_5$Se$_{10}$Cl$_2$ (A = Cs, Rb, K)	$I\bar{4}$	3.22	0.8	0.006–0.011/NPM	3D	21
Ba$_4$ZnGa$_4$Se$_{10}$Cl$_2$	$I\bar{4}$	3.08	59	0.002/NPM	3D	44
Ba$_6$Cs$_2$In$_2$Ga$_8$Se$_{20}$Cl$_4$	$I\bar{4}$	3.01	64	NPM	3D	49
Ba$_6$Cs$_2$InGa$_9$Se$_{20}$Cl$_4$	$I\bar{4}$	2.90	70	NPM	3D	49
ABa$_2$Ga$_4$S$_8$Cl (A = Rb, Cs)	$Pmn2_1$	3.35/3.30	0.9/1.0	PM	2D	20
[ABr][Hg$_2$P$_2$S$_8$] (A = Rb, Cs; X = Cl, Br)	$C222_1$	2.94–3.00	0.8–1.2	PM	2D	53 and 56
[A$_3$X][Ga$_3$PS$_8$] (A = K, Rb; X = Cl, Br)	$Pm/Pmn2_1$	3.50–3.85	1.0–2.0	PM	2D	54–56
[Rb$_4$Cl][Cd$_{11}$In$_9$S$_{26}$]	$Cmc2_1$	2.32	0.23	NPM	2D	50
Cs$_2$[Mn$_2$Ga$_3$S$_7$Cl]	$Pnma$	3.11	—	—	2D	43
Ba$_7$In$_2$Se$_6$F$_8$	$C2/m$	—	—	—	1D	51
Ba$_4$Ge$_9$S$_9$Cl$_2$	$P6_3$	2.91	2.4	NPM	0D	22
Ba$_{18}$In$_8$S$_{21}$F$_{18}$	$P4_2/ncm$	2.28	—	—	0D	52
Ba$_3$GaS$_4$Cl	$Pnma$	2.14	—	—	0D	51
NaSr$_4$ClGe$_3$S$_{10}$	$P6_3$	3.54	1.08	0.015/NPM	0D	This work
KSr$_4$ClGe$_3$S$_{10}$	$P6_3$	3.51	0.91	0.007/NPM	0D	This work
KBa$_4$ClGe$_3$S$_{10}$	$P6_3$	3.57	0.82	0.008/NPM	0D	This work

UV–Vis–Near-IR (NIR) diffuse-reflectance and IR spectra

The UV-Vis-NIR diffuse reflectance spectra were recorded in the range of 200–2000 nm using a Shimadzu SolidSpec-3700DUV spectrophotometer at room temperature. BaSO$_4$ was utilized as the standard. Absorption (K/S) data were also calculated from the following Kubelka–Munk function: $F(R) = (1 - R)^2/2R = K/S$, where R represents the reflectance, K represents the absorption, and S represents the scattering factor.[31] The IR spectra of target compounds were recorded using a Nicolet iS50 FT-IR spectrometer with ATR in the range of 2.5–25 μm at room temperature (Fig. S3†). About 5 mg of polycrystalline samples were placed on the test platform for testing.

Raman spectroscopy

Raman spectra were recorded with a powder of [ASr$_4$Cl][Ge$_3$S$_{10}$] (A = Na, K) and [KBa$_4$Cl][Ge$_3$S$_{10}$] on a confocal Raman system (WITECalpha300R) with a CCD detector using 532 nm radiation from a diode laser. The measurement range is 90–9000 cm^{-1}. The laser spot diameter is shorter than 1 μm and the test time is less than 60 s.

Powder second-harmonic generation measurement

As [ASr$_4$Cl][Ge$_3$S$_{10}$] (A = Na, K) and [KBa$_4$Cl][Ge$_3$S$_{10}$] crystallize in the noncentrosymmetric and polar structure, the powder second-harmonic generation measurement was carried out with irradiation of a 2090 nm laser by using the modified Kurtz–Perry method to evaluate the frequency conversion ability of the title compounds.[32] They were ground and sieved in the range of 54–100, 100–125, 125–150, 150–180, and 180–225 μm, respectively. And a powder AgGaS$_2$ sample with the same particle size range was used as a reference.

The details of computational methods

On the basis of density functional theory (DFT),[33] the electronic band structures, the partial density of states, and optical properties of [NaSr$_4$Cl][Ge$_3$S$_{10}$], [KSr$_4$Cl][Ge$_3$S$_{10}$], and [KBa$_4$Cl][Ge$_3$S$_{10}$] were implemented in the CASTEP package. In order to describe the exchange–correlation energy, we used a Perdew–Burke–Ernzerhof (PBE) functional in the generalized gradient approximation (GGA). The optimized norm-conserving pseudopotentials in the Kleinman–Bylander form were used to model the effective interactions between valence electrons and the atom cores. Na $2S^2 2p^6 3s^1$, K $3S^2 3p^6 4s^1$, Sr $4S^2 4p^6 5s^2$, Ba $5S^2 5p^6 6s^2$, Ge $4s^2 4p^2$, S $3s^2 3p^4$, and Cl $3s^2 3p^5$ electrons were set to be the valence electrons. The pseudopotential was set as the norm-conserving pseudopotential (NCP). The plane-wave energy cutoff value was set at 810.0 eV. And the corresponding 4 × 4 × 4 Monkhorst–Pack κ-point mesh was adopted for [NaSr$_4$Cl][Ge$_3$S$_{10}$], [KSr$_4$Cl][Ge$_3$S$_{10}$], and [KBa$_4$Cl][Ge$_3$S$_{10}$]. On the basis of the electron transition from the valence band (VB) to the conduction band (CB), we deduced the imaginary part of the dielectric function. Then, by using the Kramers–Kronig transform, we calculated the real part of the dielectric function.[34] And the refractive index n (and the birefringence Δn) was obtained from the real part of the dielectric function.

Results and discussion

Crystal structures

[NaSr$_4$Cl][Ge$_3$S$_{10}$], [KSr$_4$Cl][Ge$_3$S$_{10}$], and [KBa$_4$Cl][Ge$_3$S$_{10}$] are iso-structural and crystallize in the noncentrosymmetric and polar hexagonal space group, $P6_3$. Owing to their similar crystal structures, only the structure of [NaSr$_4$Cl][Ge$_3$S$_{10}$] will be discussed as the representative. The asymmetric unit of [NaSr$_4$Cl][Ge$_3$S$_{10}$] contains one unique Na, two Sr, one Ge, four S, and one Cl atom (s). Sr(1) and S(2) atoms are at Wyckoff sites of 2d, and Na(1) and Cl(1) atoms occupy the Wyckoff sites of 2a, while others are all at the general position 6c.

5934 | *Inorg. Chem. Front.*, 2022, **9**, 5932–5940

This journal is © the Partner Organisations 2022

All of the Ge atoms are coordinated to four S atoms to form GeS_4 tetrahedra, and three GeS_4 tetrahedra are further linked by sharing corner S atoms to generate the isolated $[Ge_3S_9]$ rings (Fig. 1a). The Cl atom is surrounded by two Na atoms and three Sr(2) atoms with Cl–Na distances of 2.910(3)–3.010 (3) Å and Cl–Sr(2) distances of 2.934(4) Å to form a $[ClNa_2Sr_3]^{7+}$ polycation secondary polyhedron, which connects to form a one-dimensional (1D) $^1_\infty[ClNaSr(2)_3]^{6+}$ chain that acts as a scissor to cut the connection between the anionic groups. All the $^1_\infty[ClNaSr(2)_3]^{6+}$ chains and $[Ge_3S_9]$ rings are alternately stacked with each other and consolidated by Sr(1)–S and Na–S ionic interactions to form a three-dimensional (3D) framework (Fig. 1c). It is interesting to note that the macroscopic packing of these $[Ge_3S_9]$ rings is arranged with the 6_3 screw shaft, along the c axis. Thus, the overall polarity of the compound from the polarity superposition of the $[Ge_3S_9]$ polar rings leads to a moderate second-harmonic generation response as discussed below.

The other complete coordination environments of cations are shown in Fig. S4 in the ESI.† The Ge–S interatomic distance ranges from 2.157(6) to 2.245(6) Å, and the S–Ge–S angle deviates from 99.60(3) to 110.30(3)° (Table S3†). The Sr(1)–S distances range from 3.045(6) to 3.057(5) Å, the Sr(2)–Cl bond length is 2.930(2) Å, and the Sr(2)–S distances range from 2.922(4) to 3.646(8) Å (Table S3†). The Na–S bond length is 2.818(5) Å, and the Na–Cl distances range from 2.910(2) to 3.010(2) Å (Table S3†). These are all consistent with the results in other compounds, such as $Ba_4Ge_3S_9Cl_2$,[22] $KBa_3Ga_5Se_{10}Cl_2$,[21] and $NaGaS_2Cl$.[35] The bond valence sum (BVS) analysis results of each atom show that the BVSs of Na, Sr, Ge, S and Cl are 0.93, 1.87–2.37, 4.21, 1.82–2.09 and 1.20, respectively (Table S2†), which are in agreement with the expected values.[36,37]

The influence of the (M + N)/Q ratios (M = IB or IIB, N = IIIA or IVA; Q = S, Se) on the chalcohalide anionic dimensions

Furthermore, as is known to all, chalcohalides have received considerable attention in IR nonlinear optical crystals due to not only their excellent properties but also their rich structural chemistry. According to Hwu's definition, chalcohalides can be observed as salt-inclusion chalcogenides which are composed of covalent chalcogenide lattices and ionic halide lat-

tices (Fig. 2).[38] The covalent chalcogenide lattices exhibit four different structural configurations from a zero-dimension (0D) to a three-dimension (3D). As shown in Fig. 3, the chalcogenide lattices in most of the reported chalcohalides (~61%) are
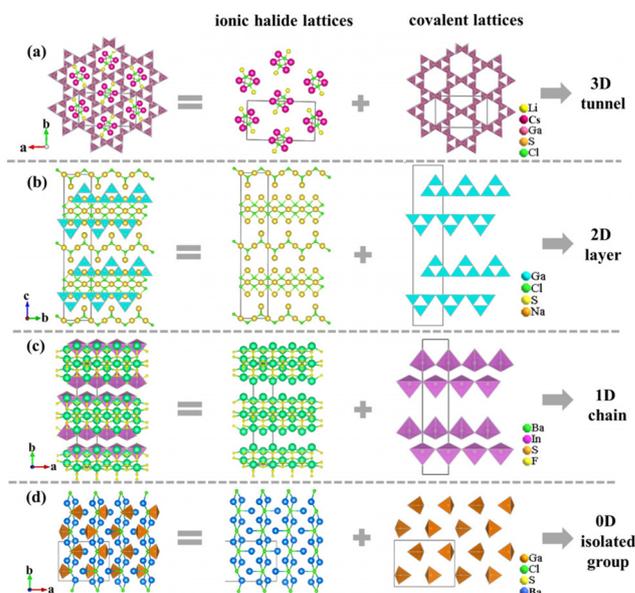

Fig. 2 Different structural configurations of covalent chalcogenide lattices in the salt-inclusion chalcogenides of $Li_2Cs_2Ga_3S_6Cl$ (a), $NaGaS_2Cl$ (b), $Ba_7In_2Se_6F_8$ (c), and Ba_3GaS_4Cl (d).
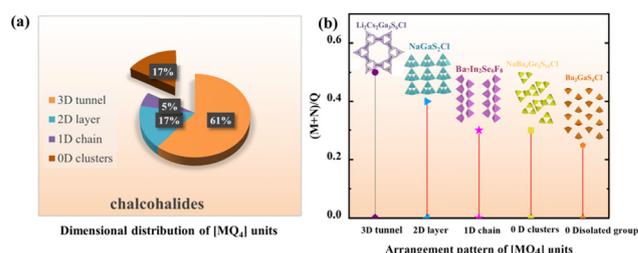

Fig. 3 Distribution of chalcohalides with specific dimensionality of the M-Q anionic framework. Inset: Corresponding proportion in % (a), and the arrangement pattern of $[MQ_4]$ units (b).
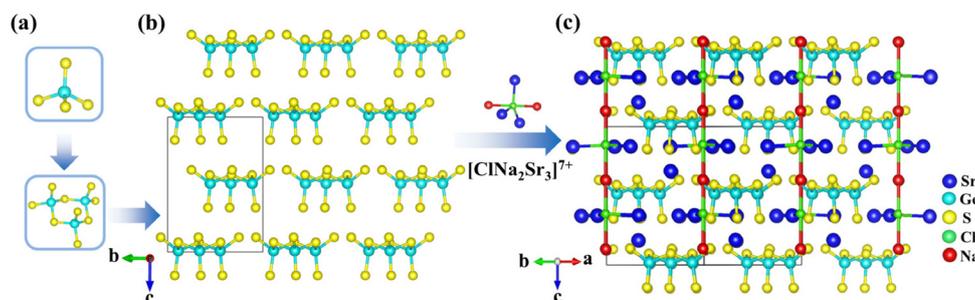

Fig. 1 Coordination environments of Ge atoms (a), arrangement of anionic groups in $[NaSr_4Cl][Ge_3S_{10}]$ (b), and $[Ge_3S_9]$ rings and $^1_\infty[ClNaSr(2)_3]^{6+}$ chains stacked along the c-axis of $[NaSr_4Cl][Ge_3S_{10}]$ (c).

This journal is © the Partner Organisations 2022

Inorg. Chem. Front., 2022, **9**, 5932–5940 | **5935**

the 3D frameworks, whereas low-dimensional chalcogenide lattices, such as 2D chalcogenide layers (17%), 1D chains (5%) or 0D clusters (17%), are rarely reported. As we know, for the chalcohalides, the covalent chalcogenide lattices made the main contribution to the second-harmonic generation responses of materials. So, the different structural configurations will have a significant effect on the materials' properties. In order to better understand the effect of composition on the different configurations of chalcogenide lattices, we carried out a further study on their structures, and some interesting rules between the structural dimensions and $(M + N)/Q$ ratios (M = IIIA or IVA, N = IB or IIB or cations coordinated as $[M_xQ_y]$ anionic groups; Q = S, Se) have been found, i.e. when $(M + N)/Q \leq 0.33$, the chalcogenide lattices tend to form 0D clusters or 1D chains, e.g. $Ba_7In_2Se_6F_8$ and Ba_3GaS_4Cl;[51] when $(M + N)/Q \geq 0.5$, they more tend to form 2D layers or 3D frameworks, e.g. $Ba_4ZnGa_4Se_{10}Cl_2$[21] and $[A_3X][Ga_3PS_8]$ (A = K, Rb; X = Cl, Br).[53–56] No chalcohalides have been reported so far in the region of $0.33 < (M + N)/Q < 0.5$ (Table S4†). The reason for the above rules can be attributed to the weak polarizability of the electron cloud of ionic bonds compared to covalent bonds. Thus the strong ionic bond can play the role of scissors to reduce the dimensionality of the framework, and the lower the content of M or N in the structure, the sparer the connection of the $M(N)Q_n$ tetrahedra will be (Fig. 2).[35] For title compounds, their $(M + N)/Q$ ratios are 0.3. Therefore, their chalcogenide lattices are 0D $[Ge_3S_9]$ clusters, which are also consistent with the above rules.

UV-Vis-NIR spectra

In order to study the optical properties, the pure polycrystalline samples of the title compounds were used to measure UV-Vis-NIR diffuse reflectance. As shown in Fig. 4, the UV cutoff edges of $[NaSr_4Cl][Ge_3S_{10}]$, $[KSr_4Cl][Ge_3S_{10}]$, and $[KBa_4Cl][Ge_3S_{10}]$ are 314, 312, and 318 nm, respectively. Correspondingly, the band gaps are 3.54, 3.51, and 3.57 eV, which are obviously larger than commercial IR nonlinear optical crystals $AgGaS_2$ (2.73 eV),[9] $AgGaSe_2$ (1.83 eV),[10] and $ZnGeP_2$ (2.34 eV),[11] and larger than most of the other chalcohalides (Table 1). Generally, the large band gap is positively related to the high laser damage threshold because the large band gap can reduce the two- or multiple-photon absorption
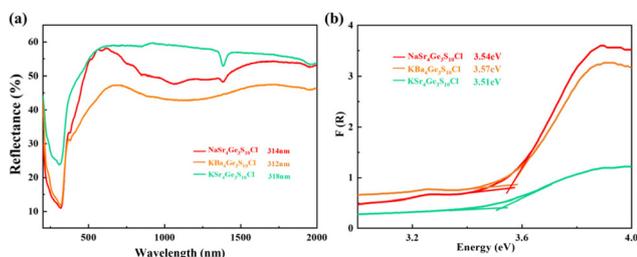
effectively.[39] And the laser damage threshold of $[ASr_4Cl][Ge_3S_{10}]$ (A = Na, K) and $[KBa_4Cl][Ge_3S_{10}]$ have also been measured based on an $Nd:Y_3Al_5O_{12}$ nanosecond laser (1064 nm, 1 Hz, 10 ns) with $AgGaS_2$ as the reference with the same particle size range of 120–150 μm. The pulse power was gradually increased and then stopped and recorded until obvious damage appeared on the sample surface. It shows that $[NaSr_4Cl][Ge_3S_{10}]$, $[KSr_4Cl][Ge_3S_{10}]$, and $[KBa_4Cl][Ge_3S_{10}]$ have high power laser damage thresholds, 223, 243, and 244 MW cm^{-2}, respectively. They are 11, 12, and 12 × $AgGaS_2$ (~20.33 MW cm^{-2}, 1064 nm, 110A, 1 Hz, 20 ns), respectively.

IR and Raman spectra

The IR spectra of $[ASr_4Cl][Ge_3S_{10}]$ (A = Na, K) and $[KBa_4Cl][Ge_3S_{10}]$ are shown in Fig. S3.† It can be seen that the title compounds have similar IR spectra. All of them have no obvious absorption in a wide range from 4000 to 400 cm^{-1} (i.e. 2.0–20 μm), which covers the two most important atmospheric transparency windows at 3–5 and 8–12 μm. Furthermore, Raman spectra were recorded (Fig. S5†). The absorption between 200 and 450 cm^{-1} can be assigned to the characteristic vibration of the Ge–S mode, and other Raman peaks below 200 cm^{-1} are due to the Ba–S or Sr–S vibrations. These are consistent with those of other related chalcogenides, such as Na_2BaGeS_4,[40] $SrCdGeS_4$,[41] and $Ba_4GaS_4F_3$.[42]

Second harmonic generation properties

To further evaluate the second-harmonic generation properties of $[ASr_4Cl][Ge_3S_{10}]$ (A = Na, K) and $[KBa_4Cl][Ge_3S_{10}]$, powder SHG measurement was also carried out under fundamental 2090 nm wavelength laser radiation by the Kurtz and Perry method with the same $AgGaS_2$ as the benchmark.[32] The second-harmonic generation intensities as a function of particle size for $[ASr_4Cl][Ge_3S_{10}]$ (A = Na, K) and $[KBa_4Cl][Ge_3S_{10}]$ and $AgGaS_2$ are shown in Fig. 5. The second-harmonic generation responses at 54–100 μm are around 1.08, 0.91, and 0.82 × $AgGaS_2$, respectively. These are equivalent to some reported IR nonlinear optical crystals, such as $ABa_3Ga_5Se_{10}Cl_2$ (A = Cs, Rb, K),[21] $ABa_2Ga_4S_8Cl$ (A = Rb, Cs),[20] and $[K_3Cl][Mn_2Ga_6S_{12}]$ (Table 1).[43] The curves of second-harmonic generation signal versus particle size (Fig. 5a) indicated the non-phase-matchable nature of the compounds in the spectral region examined. Remarkably, as shown in Fig. S1,† the Flack parameter of the
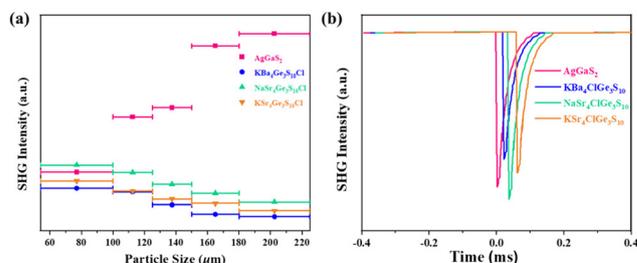

Fig. 4 UV-vis-NIR diffuse-reflectance spectrum (a), and band gaps (b) of $[NaSr_4Cl][Ge_3S_{10}]$, $[KSr_4Cl][Ge_3S_{10}]$, and $[KBa_4Cl][Ge_3S_{10}]$. (The UV-vis-NIR samples were polycrystalline samples that were synthesized by the high temperature solid phase method at 1123 K).

Fig. 5 Second-harmonic generation intensities of $[NaSr_4Cl][Ge_3S_{10}]$, $[KSr_4Cl][Ge_3S_{10}]$ and $[KBa_4Cl][Ge_3S_{10}]$ (a), and $AgGaS_2$ at a particle size of 54–100 μm (b).

5936 | *Inorg. Chem. Front.*, 2022, **9**, 5932–5940

This journal is © the Partner Organisations 2022

title compounds turns out to be quite high (0.207–0.247). This indicates that $[ASr_4Cl][Ge_3S_{10}]$ (A = Na, K) and $[KBa_4Cl][Ge_3S_{10}]$ exhibit partial twining, which may reduce the observed SHG efficiency.[44]

Birefringence measurements

Furthermore, the birefringence of $[ASr_4Cl][Ge_3S_{10}]$ (A = Na, K) and $[KBa_4Cl][Ge_3S_{10}]$ was measured using a cross-polarizing microscope in the visible region. The observed interference colors in cross-polarized light were one-order orange, one-order yellow and one-order yellow for $[NaSr_4Cl][Ge_3S_{10}]$, $[KSr_4Cl][Ge_3S_{10}]$, and $[KBa_4Cl][Ge_3S_{10}]$, respectively (Fig. S6†). On the basis of the Michel-Levy chart, the retardations (R values) were found to be 420, 300 and 310 nm, respectively. And their crystal thicknesses were found to be 19.8, 28.7, and 26.2 μm, respectively. Thus, based on the formula $R = \Delta n \times d$ (R, Δn, and d are the retardation, birefringence, and thickness, respectively), their birefringence in the visible region can be calculated as 0.02, 0.01, and 0.01 for $[NaSr_4Cl][Ge_3S_{10}]$, $[KSr_4Cl][Ge_3S_{10}]$, and $[KBa_4Cl][Ge_3S_{10}]$, respectively, which are equivalent to some reported IR nonlinear optical crystals, such as $Ba_4ZnGa_4S_{10}Cl_2$,[12] $ABa_3Ga_5Se_{10}Cl_2$ (A = Cs, Rb, K),[21] and $Ba_4ZnGa_4S_{10}Cl_2$.[45] Furthermore, their birefringence is also calculated based on the electron structures (Fig. S7†). The first-principles calculation results are consistent with our experimental values (Δn = 0.015, 0.007, and 0.008@2050 nm for $[NaSr_4Cl][Ge_3S_{10}]$, $[KSr_4Cl][Ge_3S_{10}]$, and $[KBa_4Cl][Ge_3S_{10}]$, respectively). The relatively small Δn values in the IR region indicate non-phase-matchable behaviors, which are consistent with the experimental observations.

Electronic structure calculations

In order to better understand the origin of the second-harmonic generation response, we calculated the electron structures using first-principles calculations under the same parameters. And the results show that the title compounds are direct band gaps with calculated band gaps of 2.25, 2.22, and 2.01 eV for $[NaSr_4Cl][Ge_3S_{10}]$, $[KSr_4Cl][Ge_3S_{10}]$, and $[KBa_4Cl][Ge_3S_{10}]$, respectively (Fig. S8†), which are smaller than the experimental value attributable to the discontinuity of exchange–correlation energy.[46] The partial density of states analysis of transitions from occupied states to unoccupied states reveals the microcosmic origin of the optical properties from an electronic level insight: the tops of valence bands (VBs) of $[NaSr_4Cl][Ge_3S_{10}]$ are mainly composed of S 3p, Ge 4s, and Ge 4p states, while the bottoms of the conduction bands (CBs) are primarily S 3s states (Fig. S9†). These suggest that GeS_4 tetrahedra made a major contribution to the band gap and second-harmonic generation response, as the optical properties of the material are mainly affected by electronic transitions between energy levels close to the forbidden band.

The dipole moment calculations based on the bond-valence modes

In order to understand the structural origin resulting in their functional properties, a dipole moment analysis based on the
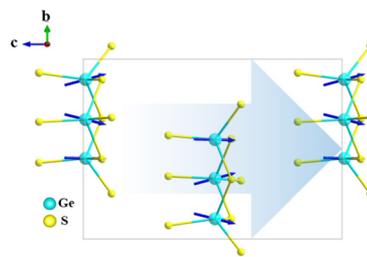

Fig. 6 The polarization direction (the blue arrow directions) of the $[Ge_3S_9]$ rings of $[NaSr_4Cl][Ge_3S_{10}]$ in a unit cell.

bond valence method has also been carried out (Table S5†). In $[ASr_4Cl][Ge_3S_{10}]$ (A = Na, K) and $[KBa_4Cl][Ge_3S_{10}]$, the $[G_3S_9]$ polyhedron has a large distortion and produces a dipole moment of 10.65–12.43 Debye, which is well consistent with our second-harmonic generation measurements. And the dipole moments of $[G_3S_9]$ rings adopt an additive arrangement manner toward the c-axis in a unit cell (Fig. 6). Therefore, the second-harmonic generation responses are mainly ascribed to the contribution of polarity superposition of the $[G_3S_9]$ polar rings.

Conclusions

In summary, a class of chalcohalides $[ASr_4Cl][Ge_3S_{10}]$ (A = Na, K) and $[KBa_4Cl][Ge_3S_{10}]$ in the noncentrosymmetric space group $P6_3$ have been synthesized through an appropriate flux method in the M/N/Ge/S/Cl system. All of the compounds feature 0D frameworks consisting of $[Ge_3S_9]$ rings arranged in the c-axis, which are isolated from each other by the 1D $^1_\infty[ClNaSr(2)_3]^{6+}$ chains. Remarkably, they not only exhibit wide E_g values (3.51–3.57 eV), and wide IR transparent window up to 20 μm, but also have moderate second-harmonic generation responses (0.82–1.08 $\times$ AgGaS$_2$). The combination of dipole moment calculation and systematic theoretical analysis reasonably explains that the second-harmonic generation responses are mainly ascribed to the contribution of polarity superposition of the $[G_3S_9]$ polar rings. Furthermore, the influence of the (M + N)/Q ratios (M = IB or IIB, N = IIIA or IVA; Q = S, Se) on the anionic group dimensions is also discussed. The results presented in the study would be of potential value for producing a general law to predict and design new high-performance IR nonlinear optical chalcohalides, and thus related non-centrosymmetric materials and studies are underway.

Author contributions

Writing – original draft: Yufei Song; review & editing: Shaoxin Cui, Zhen Qian and Hongwei Yu; resources: Zhanggui Hu; supervision: Jiyang Wang and Yicheng Wu; funding acquisition and conceptualization – ideas: Hongping Wu.

This journal is © the Partner Organisations 2022

Inorg. Chem. Front., 2022, **9**, 5932–5940 | **5937**

Conflicts of interest

There are no conflicts to declare.

Acknowledgements

References

1 U. Keller, Recent developments in compact ultrafast lasers, *Nature*, 2003, **424**, 831–838.

2 R. L. Byer, Diode laser—pumped solid-state lasers, *Science*, 1988, **239**, 742–747.

3 C. Li, X. Wang, Y. Wu, F. Liang, F. Wang, X. Zhao, H. Yu and H. Zhang, Three-dimensional nonlinear photonic crystal in naturally grown potassium-tantalate-niobate perovskite ferroelectrics, *Light: Sci. Appl.*, 2020, **9**, 193.

4 M. Shao, F. Liang, H. Yu and H. Zhang, Pushing periodic-disorder-induced phase matching into the deep-ultraviolet spectral region: theory and demonstration, *Light: Sci. Appl.*, 2020, **9**, 45.

5 X. Wang, Y. Wang, B. Zhang, F. Zhang, Z. Yang and S. Pan, CsB_4O_6F: a congruent–melting deep–ultraviolet nonlinear optical material by combining superior functional units, *Angew. Chem., Int. Ed.*, 2017, **129**, 14307–14311.

6 H. Wu, H. Yu, Z. Yang, X. Hou, X. Su, S. Pan, K. R. Poeppelmeier and J. M. Rondinelli, Designing a deep-ultraviolet nonlinear optical material with a large second harmonic generation response, *J. Am. Chem. Soc.*, 2013, **135**, 4215–4218.

7 H. Yu, H. Wu, S. Pan, Z. Yang, X. Su and F. Zhang, A novel deep UV nonlinear optical crystal $Ba_3B_6O_{11}F_2$, with a new fundamental building block, B6O14 group, *J. Mater. Chem.*, 2012, **22**, 9665–9670.

8 G. Shi, Y. Wang, F. Zhang, B. Zhang, Z. Yang, X. Hou, S. Pan and K. R. Poeppelmeier, Finding the next deep-ultraviolet nonlinear optical material: $NH_4B_4O_6F$, *J. Am. Chem. Soc.*, 2017, **139**, 10645–10648.

9 A. O. Okorogu, S. B. Mirov, W. Lee, D. I. Crouthamel, N. Jenkins, A. Y. Dergachev, K. L. Vodopyanov and V. V. Badikov, Tunable middle infrared downconversion in GaSe and $AgGaS_2$, *Opt. Commun.*, 1998, **155**, 307–312.

10 G. Boyd, H. Kasper, J. McFee and F. Storz, Linear and nonlinear optical properties of some ternary selenides, *IEEE J. Quantum Electron.*, 1972, **8**, 900–908.

11 G. Boyd, E. Buehler and F. Storz, Linear and nonlinear optical properties of $ZnGeP_2$ and CdSe, *Appl. Phys. Lett.*, 1971, **18**, 301–304.

12 H. Chen, Y.-Y. Li, B. Li, P.-F. Liu, H. Lin, Q.-L. Zhu and X.-T. Wu, Salt-Inclusion Chalcogenide $[Ba_4Cl_2][ZnGa_4S_{10}]$: Rational Design of an IR Nonlinear Optical Material with Superior Comprehensive Performance Derived from $AgGaS_2$, *Chem. Mater.*, 2020, **32**, 8012–8019.

13 X. Chen, H. Jo and K. M. Ok, Lead mixed oxyhalides satisfying all fundamental requirements for high–performance mid–infrared nonlinear optical materials, *Angew. Chem., Int. Ed.*, 2020, **132**, 7584–7590.

14 H. Zhang, M. Zhang, S. Pan, X. Dong, Z. Yang, X. Hou, Z. Wang, K. B. Chang and K. R. Poeppelmeier, $Pb_{17}O_8Cl_{18}$: A Promising IR Nonlinear Optical Material with Large Laser Damage Threshold Synthesized in an Open System, *J. Am. Chem. Soc.*, 2015, **137**, 8360–8363.

15 X. Chen, Q. Jing and K. M. Ok, $Pb_{18}O_8Cl_{15}I_5$: A Polar Lead Mixed Oxyhalide with Unprecedented Architecture and Excellent Infrared Nonlinear Optical Properties, *Angew. Chem., Int. Ed.*, 2020, **59**, 20323–20327.

16 Y. Tsujimoto, C. A. Juillerat, W. Zhang, K. Fujii, M. Yashima, P. S. Halasyamani and H.-C. zur Loye, Function of Tetrahedral ZnS_3O Building Blocks in the Formation of $SrZn_2S_2O$: A Phase Matchable Polar Oxysulfide with a Large Second Harmonic Generation Response, *Chem. Mater.*, 2018, **30**, 6486–6493.

17 B.-W. Liu, X.-M. Jiang, G.-E. Wang, H.-Y. Zeng, M.-J. Zhang, S.-F. Li, W.-H. Guo and G.-C. Guo, Oxychalcogenide $BaGeOSe_2$: Highly Distorted Mixed-Anion Building Units Leading to a Large Second-Harmonic Generation Response, *Chem. Mater.*, 2015, **27**, 8189–8192.

18 J. Wang, Y. Cheng, H. Wu, Z. Hu, J. Wang, Y. Wu and H. Yu, $Sr_3[SnOSe_3][CO_3]$: A Heteroanionic Nonlinear Optical Material Containing Planar pi-conjugated $[CO_3]$ and Heteroleptic $[SnOSe_3]$ Anionic Groups, *Angew. Chem., Int. Ed.*, 2022, **61**, e202201616.

19 R. Wang, F. Liang, F. Wang, Y. Guo, X. Zhang, Y. Xiao, K. Bu, Z. Lin, J. Yao, T. Zhai and F. Huang, $Sr_6Cd_2Sb_6O_7S_{10}$: Strong SHG Response Activated by Highly Polarizable Sb/O/S Groups, *Angew. Chem., Int. Ed.*, 2019, **58**, 8078–8081.

20 B. W. Liu, X. M. Jiang, H. Y. Zeng and G. C. Guo, $[ABa_2Cl][Ga_4S_8]$ (A = Rb, Cs): Wide-Spectrum Nonlinear Optical Materials Obtained by Polycation-Substitution-Induced Nonlinear Optical (NLO)-Functional Motif Ordering, *J. Am. Chem. Soc.*, 2020, **142**, 10641–10645.

21 P. Yu, L. J. Zhou and L. Chen, $Ba_3AGa_5Se_{10}Cl_2$ (A = Cs, Rb, K) Noncentrosymmetric inorganic open-framework chalcohalides with strong middle IR SHG and red emission: Ba3AGa5Se10Cl2 (A = Cs, Rb, K), *J. Am. Chem. Soc.*, 2012, **134**, 2227–2235.

22 P. F. Liu, Y. Y. Li, Y. J. Zheng, J. S. Yu, R. H. Duan, H. Chen, H. Lin, L. Chen and L. M. Wu, Tailored synthesis of nonlinear optical quaternary chalcohalides: $Ba_4Ge_3S_9Cl_2$, $Ba_4Si_3Se_9Cl_2$ and $Ba_4Ge_3Se_9Cl_2$, *Dalton Trans.*, 2017, **46**, 2715–2721.

23 Y. Zhang, H. Wu, Z. Hu, J. Wang, Y. Wu and H. Yu, Achieving a strong second harmonic generation response and a wide band gap in a Hg-based material, *Inorg. Chem. Front.*, 2022, **9**(16), 4075–4080.

24 B. Liu, X. Jiang, S. Pei, W. Chen, L. Yang and G. C. Guo, *Mater. Horiz.*, 2021, **8**, 3394–3398.

25 K. Feng, L. Kang, Z. Lin, J. Yao and Y. Wu, Noncentrosymmetric chalcohalide $NaBa_4Ge_3S_{10}Cl$ with large band gap and IR NLO response, *J. Mater. Chem. C*, 2014, **2**, 4590–4596.

26 W. Zhou, Z.-H. Shi, W. Liu and S.-P. Guo, Noncentrosymmetric chalcohalide $K_2Ba_3Ge_3S_9Cl_2$: A new nonlinear optical material with remarkable laser-induced damage threshold, *J. Alloys Compd.*, 2022, **895**, 162602.

27 H. Yu, W. Zhang, J. Young, J. M. Rondinelli and P. S. Halasyamani, Bidenticity-Enhanced Second Harmonic Generation from Pb Chelation in $Pb_3Mg_3TeP_2O_{14}$, *J. Am. Chem. Soc.*, 2016, **138**, 88–91.

28 G. M. Sheldrick, SHELXT- Integrated Space-group and Crystal-structure Determination, *Acta Crystallogr., Sect. A: Found. Adv.*, 2015, **71**, 3–8.

29 G. M. Sheldrick and G. M. Sheldrick, *Acta Crystallogr., Sect. A: Found. Crystallogr.*, 2008, **64**, 112.

30 A. Spek, Single-crystal structure validation with the program PLATON, *J. Appl. Crystallogr.*, 2003, **36**, 7–13.

31 J. Tauc, Absorption edge and internal electric fields in amorphous semiconductors, *Mater. Res. Bull.*, 1970, **5**, 721–729.

32 S. Kurtz and T. Perry, A powder technique for the evaluation of nonlinear optical materials, *J. Appl. Phys.*, 1968, **39**, 3798–3813.

33 S. J. Clark, M. D. Segall, C. J. Pickard, P. J. Hasnip, M. I. Probert, K. Refson and M. C. Payne, First principles methods using CASTEP, *Z. Kristallogr. – Cryst. Mater.*, 2005, **220**, 567–570.

34 H. J. Monkhorst and J. D. Pack, Special Points for Brillouin-zone Integrations, *Phys. Rev. B: Solid State*, 1976, **13**, 5188–5192.

35 X. Li, F. Liang, T. Liu and H. Li, Na_2GaS_2Cl: a new sodium-rich chalcohalide with two-dimensional $[GaS_2]$ infinity layers and wide interlayer space, *Dalton Trans.*, 2021, **50**, 11167–11172.

36 D. Altermatt, Bond-Valence Parameters Obtained from a Systematic Analysis of the Inorganic Crystal Structure Database, *Acta Crystallogr., Sect. B: Struct. Sci.*, 1985, **41**, 244–247.

37 N. Brese and M. O'keeffe, Bond-valence parameters for solids, *Acta Crystallogr., Sect. B: Struct. Sci.*, 1991, **47**, 192–197.

38 J. P. West and S.-J. Hwu, Noncentrosymmetric salt inclusion oxides: Role of salt lattices and counter ions in bulk polarity, *J. Solid State Chem.*, 2012, **195**, 101–107.

39 T. Walker, A. Guenther and P. Nielsen, Pulsed laser-induced damage to thin-film optical coatings-Part II: Theory, *IEEE J. Quantum Electron.*, 1981, **17**, 2053–2065.

40 K. Wu, Z. Yang and S. Pan, Na_2BaMQ_4 (M=Ge, Sn; Q=S, Se): Infrared Nonlinear Optical Materials with Excellent Performances and that Undergo Structural Transformations, *Angew. Chem., Int. Ed.*, 2016, **55**, 6713–6715.

41 Y. Dou, Y. Chen, Z. Li, A. K. Iyer, B. Kang, W. Yin, J. Yao and A. Mar, $SrCdGeS_4$ and $SrCdGeSe_4$: Promising Infrared Nonlinear Optical Materials with Congruent-Melting Behavior, *Cryst. Growth Des.*, 2019, **19**, 1206–1214.

42 H. Gao, R. Chen, K. Zhang, A. Abudurusuli, K. Lai and J. Li, $Ba_4GaS_4F_3$ Synthesis, characterization and theoretical investigation of a new chalcohalide, $Ba_4GaS_4F_3$, *Dalton Trans.*, 2021, **50**, 6315–6320.

43 Y. J. Zheng, Y. F. Shi, C. B. Tian, H. Lin, L. M. Wu, X. T. Wu and Q. L. Zhu, An unprecedented pentanary chalcohalide with Mn atoms in two chemical environments: unique bonding characteristics and magnetic properties, *Chem. Commun.*, 2018, **55**, 79–82.

44 P. A. Maggard, T. S. Nault, C. L. Stern and K. R. Poeppelmeier, Alignment of Acentric $MoO_3F_3^{3-}$ Anions in a Polar Material: $(Ag_3MoO_3F_3)(Ag_3MoO_4)Cl$, *J. Solid State Chem.*, 2003, **175**, 27–33.

45 Y.-Y. Li, P.-F. Liu, L. Hu, L. Chen, H. Lin, L.-J. Zhou and L.-M. Wu, Strong IR NLO Material $Ba_4MGa_4Se_{10}Cl_2$: Highly Improved Laser Damage Threshold via Dual Ion Substitution Synergy, *Adv. Opt. Mater.*, 2015, **3**, 957–966.

46 R. Godby, M. Schlüter and L. Sham, Accurate exchange-correlation potential for silicon and its discontinuity on addition of an electron, *Phys. Rev. Lett.*, 1986, **56**, 2415.

47 B. W. Liu, X. M. Jiang, B. X. Li, H. Y. Zeng and G. C. Guo, Li $[LiCs_2Cl][Ga_3S_6]$: A Nanoporous Framework of GaS_4 Tetrahedra with Excellent Nonlinear Optical Performance, *Angew. Chem., Int. Ed.*, 2020, **59**, 4856–4859.

48 B.-W. Liu, H.-Y. Zeng, X.-M. Jiang and G.-C. Guo, Phase Matching Achieved by Bandgap Widening in Infrared Nonlinear Optical Materials $[ABa_3Cl_2][Ga_5S_{10}]$ (A = K, Rb, and Cs), *CCS Chem.*, 2021, **3**, 964–973.

49 Y.-Y. Li, P.-F. Liu, H. Lin, M.-T. Wang and L. Chen, The effect of indium substitution on the structure and NLO properties of $Ba_6Cs_2Ga_{10}Se_{20}Cl_4$, *Inorg. Chem. Front.*, 2016, **3**, 952–958.

50 S.-M. Pei, L.-T. Jiang, B.-W. Liu and G.-C. Guo, A new salt-inclusion chalcogenide exhibiting distinctive $[Cd_{11}In_9S_{26}]^{3-}$ host framework and decent nonlinear optical performances, *J. Alloys Compd.*, 2022, **902**, 163656.

51 K. Feng, W. Yin, Z. Lin, J. Yao and Y. Wu, Five new chalcohalides, Ba_3GaS_4X (X = Cl, Br), Ba_3MSe_4Cl (M = Ga, In), and $Ba_7In_2Se_6F_8$: syntheses, crystal structures, and optical properties, *Inorg. Chem.*, 2013, **52**, 11503–11508.

52 Z.-Z. Luo, C.-S. Lin, W.-L. Zhang, H. Zhang, Z.-Z. He and W.-D. Cheng, $Ba_{18}F_{18}In_8S_{21}$ and $Ba_9F_{10}In_4S_{10}$: new kind of mixed anion compounds with the novel low-dimensional structure, *CrystEngComm*, 2014, **16**, 2788–2794.

53 W. Xing, C. Tang, N. Wang, C. Li, E. Uykur, J. Wu, Z. Lin, J. Yao, W. Yin and B. Kang, $AXHg_3P_2S_8$ (A = Rb, Cs; X = Cl, Br): New Excellent Infrared Nonlinear Optical Materials with Mixed-Anion Chalcohalide Groups of Trigonal Planar $[HgS_2X]^{3-}$ and Tetrahedral $[HgS_3X]^{5-}$, *Adv. Opt. Mater.*, 2021, **9**, 2100563.

54 B. W. Liu, H. Y. Zeng, X. M. Jiang, G. E. Wang, S. F. Li, L. Xu and G. C. Guo, $[A_3X][Ga_3PS_8]$ (A = K, Rb; X = Cl, Br):

This journal is © the Partner Organisations 2022

Inorg. Chem. Front., 2022, **9**, 5932–5940 | **5939**

promising IR non-linear optical materials exhibiting concurrently strong second-harmonic generation and high laser induced damage thresholds, *Chem. Sci.*, 2016, **7**, 6273–6277.

55 Q. G. Yue, W. B. Wei, H. Chen, X. T. Wu, H. Lin and Q. L. Zhu, Salt-inclusion chalcogenides: an emerging class of IR nonlinear optical materials, *Dalton Trans.*, 2020, **49**, 14338–14343.

56 H. Lin, W.-B. Wei, H. Chen, X.-T. Wu and Q.-L. Zhu, Rational design of infrared nonlinear optical chalcogenides by chemical substitution, *Coord. Chem. Rev.*, 2020, **406**, 213150.